Supporting Information for

Identifying Key Mononuclear Fe Species for the Low-Temperature Methane Oxidation

Tao Yu,[a,b] Zhi Li,[c] Wilm Jones,[d] Yuanshuai Liu,[e] Qian He,[f] Weiyu Song,[c] Pengfei Du,[b,g] Bing Yang,[g] Hongyu An,[e] Daniela M. Farmer,[d] Chengwu Qiu,[d] Aiqin Wang,[a,h] Bert M. Weckhuysen,[e,*] Andrew M. Beale[d,*] & Wenhao Luo[a,*]

[a] CAS Key Laboratory of Science and Technology on Applied Catalysis, Dalian Institute of Chemical Physics, Chinese Academy of Sciences, 457 Zhongshan Road, Dalian,116023, China.

[b] University of Chinese Academy of Sciences, Beijing 100049, China.

[c] State Key Laboratory of Heavy Oil Processing, China University of Petroleum, Beijing 102249, China.

[d] Department of Chemistry, University College London, 20 Gordon Street, London WC1H 0AJ, UK & Research Complex at Harwell (RCaH), Rutherford Appleton Laboratory, Harwell, Didcot, Oxon OX11 0FA, UK.

[e] Inorganic Chemistry and Catalysis group, Debye Institute for Nanomaterials Science, Utrecht University, Universiteitsweg 99, Utrecht, 3584 CG, The Netherlands.

[f] Department of Materials Science and Engineering, National University of Singapore, Engineering Drive 1, Singapore, 117575, Singapore.

[g] Dalian National Laboratory for Clean Energy, Dalian Institute of Chemical Physics, Chinese Academy of Sciences, 457 Zhongshan Road, Dalian, 116023, China.

[h] State Key Laboratory of Catalysis, Dalian Institute of Chemical Physics, Chinese Academy of Sciences, Dalian 116023, China.

* Corresponding author E-mail: B.M.Weckhuysen@uu.nl, andrew.beale@ucl.ac.uk, w.luo@dicp.ac.cn.

Experimental Section

1. Catalyst preparation

All the Fe/ZSM-5 zeolites were prepared via a wet impregnation method. The required amount of H-ZSM-5 (Si/Al = 13.5, Nankai University Catalyst Co.) was charged into a 50 mL round bottom flask equipped with a magnetic stirrer. The flask was then submerged in a 30 °C oil bath and the powder was then agitated constantly. The required amount $(2.1 \text{ mL·g}^{-1}_{ZSM-5})$ of precursor solution, prepared with dissolving the requisite amount of iron (III) nitrate nonahydrate $(Fe(NO_3)_3·9H_2O, > 98\%, \text{Aladdin})$ in deionized water, was then added slowly and carefully for nearly 15 min. After complete solution addition, the slurry was stirred vigorously and then kept at 30 °C overnight. The obtained material was then dried at 110 °C in an oven with a heating ramp of 2 °C/min for 6 h. After being fully ground, the powder was calcined in a furnace at 500 °C with a heating ramp of 5 °C/min for 4 h in air. The obtained catalysts were denoted as x%Fe/ZSM-5 (x refers to the weight percentage).

2. Catalyst testing

The methane oxidation reaction was conducted in a 160 mL Parr autoclave reactor (Model 4792). The vessel was loaded with an aqueous solution of H_2O_2 (80 mL, 0.5 M) and 0.3 g catalyst, purged three times with methane and charged with methane to 30 bar. The reaction mixture was heated to the desired temperature (50 °C) with a slow stirring speed of 200-300 rpm. Once the desired temperature was achieved, the stirring speed was raised to 1500 rpm, which was taken as the starting point of the reaction. After the reaction was finished, the vessel was quickly cooled in an ice water bath. The reaction products were identified by ^{13}C nuclear magnetic resonance (NMR) and quantified by ^{1}H NMR on a 400 MHz Bruker AVANCE III NMR spectrometer. ^{13}C NMR spectra were acquired with a $\pi/6$ pulse width of 10 μs, a recycle delay of 2 s, and 1024 scans. ^{1}H NMR spectra were recorded with a $\pi/2$ pulse width of 10 μs, a recycle delay of 5 s, and 20 scans. Typically, 490 μL of sample, 100 μL of D_2O and 10 μL internal standard (1% acetonitrile aqueous solution) were placed in an NMR tube together. A solvent suppression program was run in order to minimize the signal arising from solvent. The 2D ^{1}H-^{13}C heteronuclear multiple quantum correlation (HMQC) experiment was performed on a 700 MHz Bruker AVANCE III HD set-up and collected with [1024/128] complex points in the (^{1}H/^{13}C) dimensions and corresponding acquisition times of [73 ms/1.9 ms]. A recycle delay of 2 s was used along with 8 scans. The gas phase reaction products were analyzed by a PANNA A91 GC equipped with TDX-01 and Porapak Q columns and thermal conductivity detector (TCD).

3. Catalyst stability testing

The stability tests were performed under the applied conditions as mentioned in the Catalyst testing section. Three consecutive runs were conducted in a 160 mL Parr autoclave reactor (Model 4792) at 50 °C for 30 min with an 80 mL aqueous solution of 0.5 M H_2O_2, 30 bar methane and 0.3 g catalyst. After each reaction, the catalyst was separated from the reaction mixture by centrifugation, filtration and washed with water, and then dried at 80 °C for 4 h. Parallel tests were carried out for each cycle, to guarantee enough of the spent catalyst for a consecutive run. The obtained powder was submitted to the consecutive run.

4. Methanol oxidation testing

The methanol oxidation reaction was performed under the same condition as mentioned in the Catalyst testing part

except that 0.2 mL methanol was dropped into the 0.5 M H_2O_2 aqueous solution and the autoclave was charge with pure nitrogen. The reaction products were identified by ^{13}C NMR.

5. *Ex situ* catalyst characterization methods

X-ray diffraction (XRD) analysis was carried out on a PANalytical X'pert Pro diffractometer using nickel-filtered Cu Kα radiation with a scanning angle (2 theta) of 5-60°, operated at 40 kV and 40 mA.

The metal loadings of the catalysts were determined by inductively coupled plasma optical emission spectroscopy (ICP-OES) on an Optima 7300DV instrument (PerkinElmer Instrument Corporation). Before analysis, a proper amount of powder sample was treated by hot hydrofluoric acid to obtain a clear solution.

Nitrogen physisorption measurements were conducted to determine the surface areas and pore volumes on a Micromeritics ASAP 2460 apparatus operating at -196 °C. The samples were outgassed at 300 °C under vacuum for 4 h prior to the measurements. Brunauer-Emmett-Teller (BET) surface areas were determined by the adsorption isotherm within the pressure range $0.05 < P/P_0 < 0.3$. Micropore volumes were determined by t-plot analysis, and pore size distribution was obtained from the adsorption isotherm using the Barrett-Joyner-Halenda (BJH) method.

H_2 temperature-programmed reduction (H_2-TPR) experiments were conducted on a Micromeritics AutoChem II 2920 equipped with a TCD detector. Before the reduction, about 100 mg of the sample was loaded into a U-shape quartz reactor and then treated at 300 °C under Ar flow (15 mL/min) for 1 h. After cooling to 50 °C, the flowing gas was switched to a 10% H_2/Ar gas flow, and the sample was heated to 900 °C with a ramping rate of 10 °C/min.

UV-visible (UV-vis) spectra of zeolite Fe/ZSM-5 catalysts were recorded on a Lambda950 spectrometer in the diffuse reflectance (DR) mode at room temperature. The baseline was corrected using $BaSO_4$ as a reference material. Samples were scanned between 190 and 800 nm at a scan rate of 200 nm/min. The intensity of the UV-vis DR spectra was presented in the form of the Kubelka-Munk function.

Fourier transform infrared (FT-IR) spectra of CO absorbed were recorded on a Perkin-Elmer 2000 spectrometer, measured in a transmission mode with each spectrum consisting of 25 scans at a resolution of 4 cm^{-1}. Catalyst wafers were made and loaded inside a synchrotron cell with a CaF_2 window.[1] The cell was first evacuated to 10^{-6} mbar and the sample was subsequently dried at 300 °C (3 °C/min) for 1 h. Then the cell was further cooled down to -190 °C with liquid nitrogen and connected to a gas chamber that permitted adjustment of the CO pressure injected into the cell. CO adsorption was studied at -190 °C and stepwise increasing pressures with the catalyst wafer.

Aberration-corrected scanning transmission electron microscopy (AC-STEM) imaging of the zeolite Fe/ZSM-5 catalysts was performed with a JEM ARM200F (JEOL, Japan) instrument, which is a thermal-field emission microscope with a probe Cs-corrector, and the work voltage is 200 kV. For the HAADF (High Angle Annular Dark Field) images, the convergence angle of ~23 mrad and collection angle range of 68~174 mrad were adapted for the atomic images. The elemental composition and distribution were analyzed on the energy dispersive X-ray analyzer (EX-230 100 m^2 detector) equipped on the electronic microscope.

^{57}Fe Mössbauer spectra of the zeolite Fe/ZSM-5 catalysts were measured on a Topologic 500A spectrometer at

room temperature. The radioactive source was ^{57}Co (Rh) moving in a constant acceleration mode. Velocity calibration was carried out at room temperature using an α-Fe foil. Spectra were collected with 1,024 points and summed up to 512 points. Data analysis involved a curve fitting procedure made by assuming a Lorentzian line shape and employing the fitting program MössWin 4.0. The components of iron species were identified based on their Mössbauer parameters, including isomer shift (IS) and quadruple splitting (QS). In order to get better results, samples with low iron concentrations are prepared from enriched ^{57}Fe.

6. *In situ* catalyst characterization methods

In situ X-ray absorption fine structure (XAFS) measurements of the zeolite Fe/ZSM-5 catalysts were carried out at the Diamond Light Source (Harwell Campus, UK) at the scanning branch of I20 beamline equipped with an Si (111) Scanning Four Bounce monochromator for selecting the incident X-rays energy for the Fe K edge (6980-7500 eV). The 0.1%Fe/ZSM-5 catalyst was measured under flowing gas using a heated borosilicate capillary (O.D. from 1 to 0.4 mm) as the microreactor. A sieve fraction (75-125 μm) of the sample was fixed in the capillary using quartz wool. Firstly, the catalyst was activated and dehydrated by heating at 300 °C for 1 h under 20% O_2/He flow (30 ml/min) with a heating rate of 5 °C /min, then the sample was cooled down to 50 °C in He (30 ml/min). Once the temperature reached to 50 °C, 5% CH_4/He (30 ml/min) was flown through the reactor. Normalisation and X-ray Absorption Near Edge Structure (XANES) data processing were carried out using IFEFFIT[2] with the Horae package[3] (Athena and Artemis).

In situ UV-vis diffuse reflectance (DR) spectroscopy measurements of the zeolite Fe/ZSM-5 catalysts were carried out on a Lambda950 spectrometer equipped with a home-built operando cell with quartz windows. The sample was first heated at 300 °C for 1 h under Ar flow (20 ml/min), heating at a rate of 10 °C /min, then cooled down to 50 °C. Subsequently, 10% CH_4/He (10 ml/min) was introduced to the sample for 1 h and then a small amount of 0.5 M H_2O_2 aqueous solution was dropped on the surface of sample, followed by drying under Ar at 50 °C for 1 h. The baseline was corrected using $BaSO_4$ as a reference material. The UV-vis DR spectra were collected after different treatments. Samples were scanned between 190 and 800 nm at a scan rate of 200 nm/min. The intensity of the UV-vis DR spectra was presented in the form of the Kubelka-Munk function.

In situ Fourier transform-infrared (FT-IR) spectra of the zeolite Fe/ZSM-5 catalysts were recorded on a VERTEX 70V infrared spectrometer equipped with a mercury cadmium telluride (MCT) detector and an operando cell with a ZnSe window. Optical absorption was measured in the range of 400 to 4000 cm^{-1} with a resolution of 4 cm^{-1}. Prior to being examined, 5 mg of samples were loaded into the sample cell and dehydrated at 300 °C under vacuum condition for 1 h. Pure methane was introduced with stepwise increase in pressure at 50 °C. Transmission FT-IR spectra of species were obtained by subtraction of pre-treated sample. For spectral treatment the OPUS software was used.

7. Calculation the average TORs of different Fe species

Three Fe species (mononuclear Fe species, oligomeric Fe_xO_y clusters and Fe_2O_3 nanoparticles) can be discriminated by the UV-vis and Mössbauer spectroscopy. According to the respective fractions of Mössbauer spectra (Table S3), the average TOR of different Fe species, can be calculated with the equation:

$$TOR = \frac{Number\ of\ methanol\ moleculers}{Number\ of\ Fe\ atoms\ \times\ reaction\ time}$$

The average activity of different active species, denoted as $TOR_{monomer}$, $TOR_{oligomer}$ and $TOR_{particle}$, can be calculated with these equations:

$$TOR_{0.1\%Fe} = TOR_{monomer}\ \times\ Area_{monomer}\%\ +\ TOR_{oligomer}\ \times\ Area_{oligomer}\%$$

$$TOR_{0.5\%Fe} = TOR_{monomer}\ \times\ Area_{monomer}\%\ +\ TOR_{oligomer}\ \times\ Area_{oligomer}\%\ +\ TOR_{particle}\ \times\ Area_{particle}\%$$

$$TOR_{2\%Fe} = TOR_{monomer}\ \times\ Area_{monomer}\%\ +\ TOR_{oligomer}\ \times\ Area_{oligomer}\%\ +\ TOR_{particle}\ \times\ Area_{particle}\%$$

$\rightarrow$

$$TOR_{monomer}\ \times\ 66\%\ +\ TOR_{oligomer}\ \times\ 34\% = 66$$

$$TOR_{monomer}\ \times\ 43\%\ +\ TOR_{oligomer}\ \times\ 42\%\ +\ TOR_{particle}\ \times\ 15\% = 15$$

$$TOR_{monomer}\ \times\ 28\%\ +\ TOR_{oligomer}\ \times\ 57\%\ +\ TOR_{particle}\ \times\ 15\% = 4$$

$\rightarrow$

$$TOR_{monomer}\ = 90.9$$

$$TOR_{oligomer}\ = 17.6$$

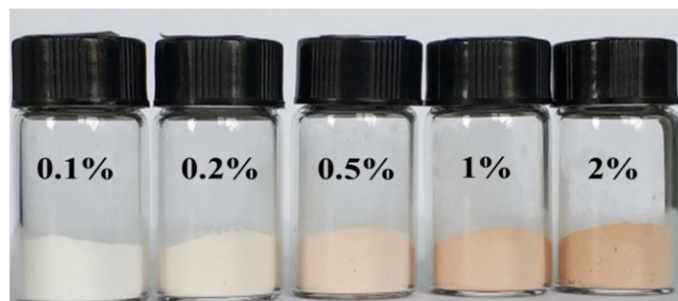$$TOR_{particle}\ = -209.9$$

Figures

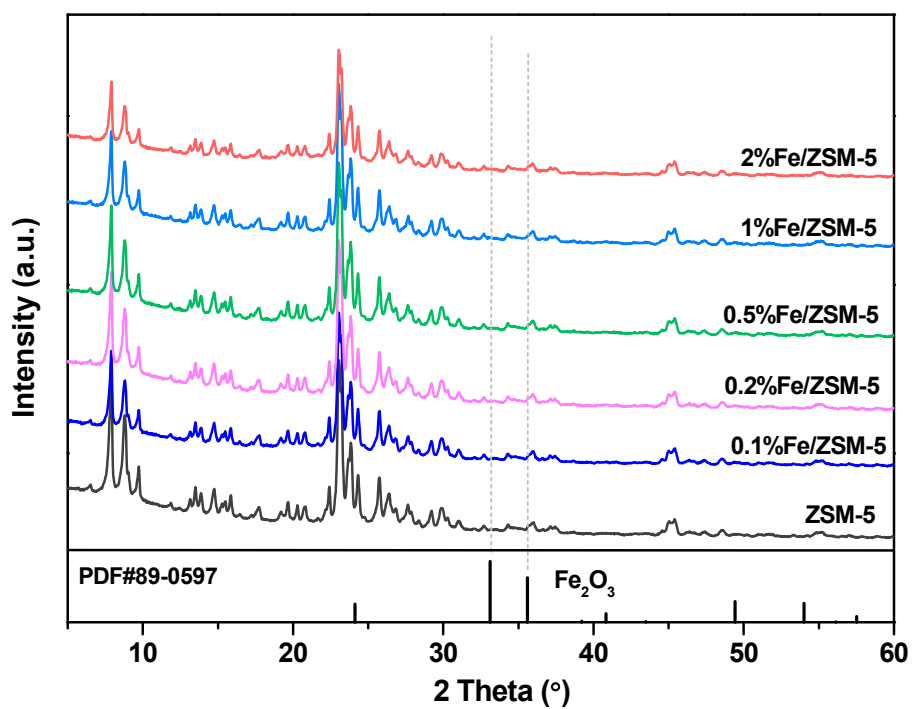**Figure S1.** The visual appearance of Fe/ZSM-5 catalysts with different Fe loadings.

Figure S2. X-ray diffraction (XRD) patterns of parent ZSM-5 and Fe/ZSM-5 catalysts. The standard XRD pattern of hematite (α-Fe_2O_3) is added for comparison. The XRD patterns of different catalysts showed no evidence for formation of new phases other than ZSM-5, indicating a good dispersion of Fe-related species.
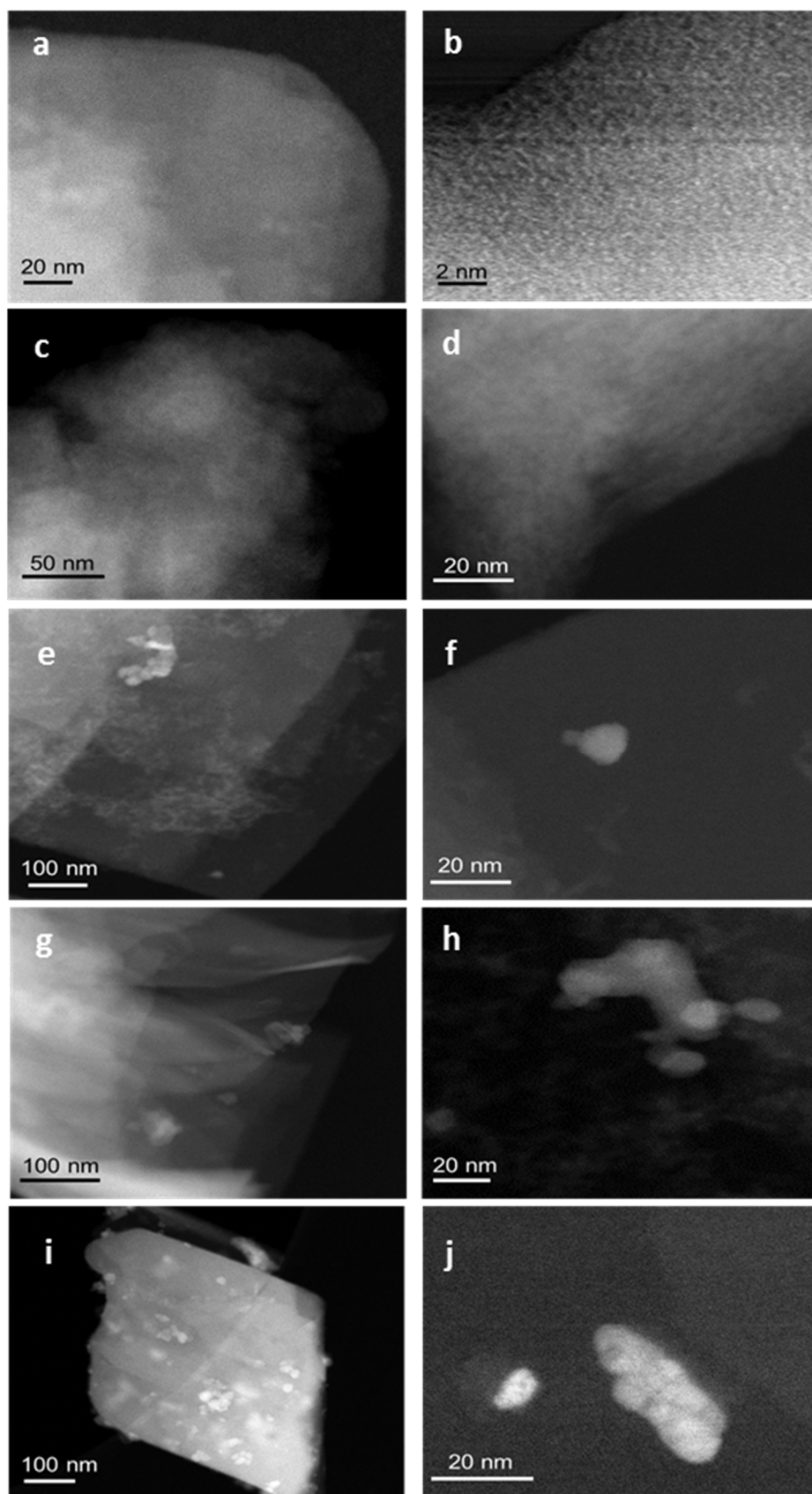
Figure S3. Representative HAADF-STEM images of the (**a**,**b**) 0.1%Fe/ZSM-5, (**c**,**d**) 0.2%Fe/ZSM-5, (**e**,**f**) 0.5%Fe/ZSM-5, (**g**,**h**) 1%Fe/ZSM-5 and (**i**,**j**) 2%Fe/ZSM-5.
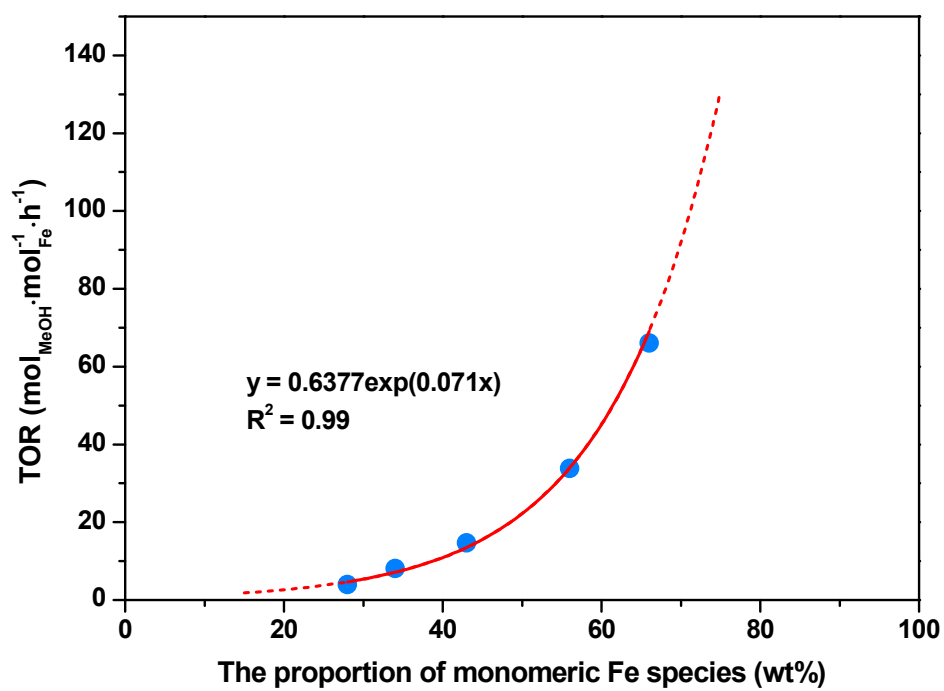
Figure S4. Correlation between the normalized TORs of five Fe/ZSM-5 zeolites and the relative proportion of monomeric Fe species, quantified through the ^{57}Fe Mössbauer spectra.
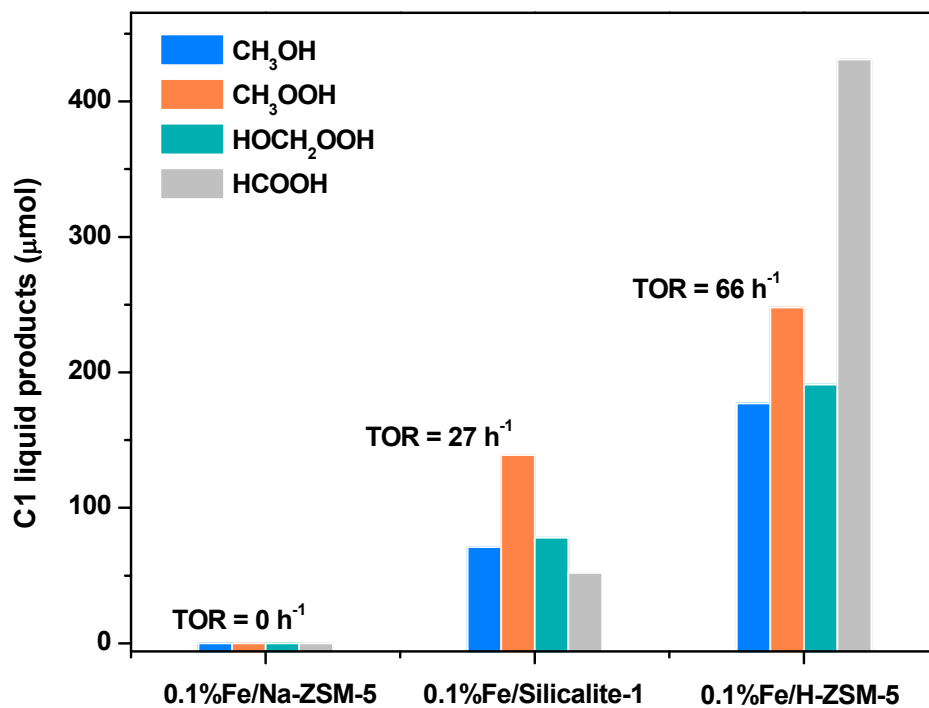
Figure S5. The catalytic performance of methane oxidation by the 0.1%Fe/Na-ZSM-5, 0.1%Fe/Silicalite-1 and 0.1%Fe/H-ZSM-5. Reaction conditions: T = 50 °C, P_{CH4} = 30 bar, H_2O_2 = 0.5 M, V = 80 mL, catalyst = 0.3 g, rpm = 1500, t = 30 min. (Methanol TORs are in the unit of $mol_{MeOH} \cdot mol^{-1}_{Fe} \cdot h^{-1}$)
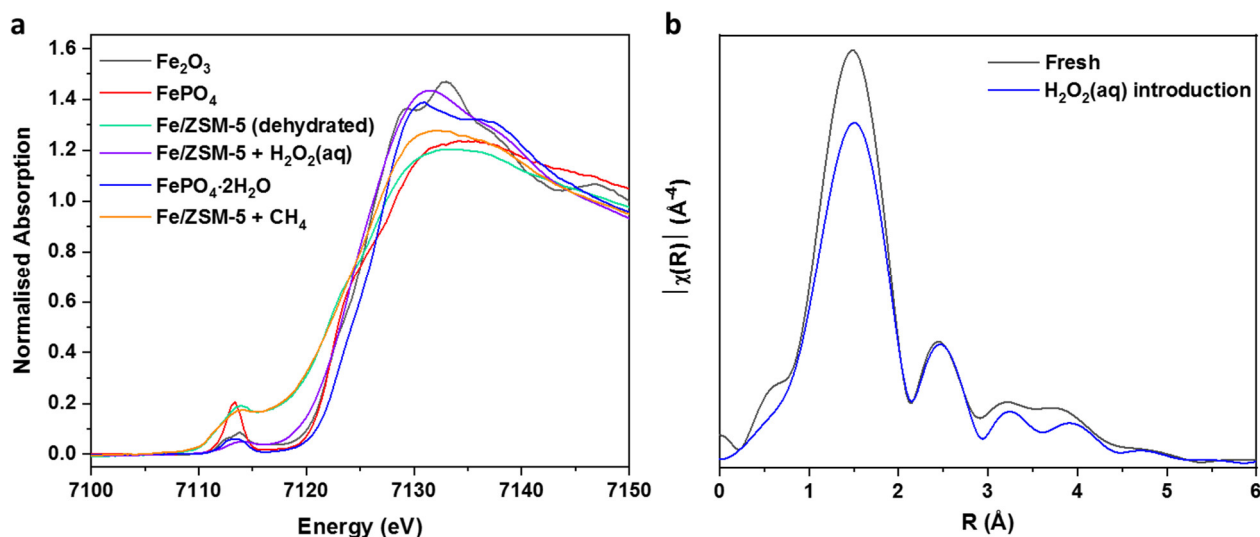
Figure S6. (**a**) XANES results of 0.1%Fe/ZSM-5 samples after undergoing various treatments. The XANES spectra of Fe_2O_3, $FePO_4$ and $FePO_4\cdot2H_2O$ were added for comparison. (**b**) *In situ* Fe K-edge EXAFS result during the interaction of fresh 0.1%Fe/ZSM-5 with H_2O_2(aq) at 50 °C.

Note: Shown in Fig. S6a is the X-ray Absorption Near Edge Structure (XANES) data recorded at the Fe K-edge for the 0.1%Fe/ZSM-5 samples after undergoing various treatments and a series of model compounds. These parts of the spectra are well-known for providing information on the electronic state and local site symmetry of Fe species. The pre-edge region weak peaks centered around ~7113 eV is due primarily to a 1s-3d transition and are indicative of compounds containing Fe species in low oxidation state (i.e. 2+ or 3+) and/or possess high site symmetry (i.e. Oh which possesses inversion symmetry). Increasing intensity of these peaks tends to be consistent with an increased oxidation state and lowering of the coordination symmetry (i.e. has no inversion symmetry), with Td. Fe^{3+} often possessing the highest intensity in a series of model compounds. Interestingly, the pre-edge XANES intensity for the dehydrated sample, is unusually intense being some ~ 3 times greater than that seen for the Oh. containing Fe^{3+} and on par (intensity-wise) with that seen for Td. Fe^{3+}. A possible explanation for this change includes a further change in symmetry (again to a site lacking inversion symmetry but not Td.,) else an increase in Fe oxidation state to Fe^{4+}. The change in the centroid position of this pre-edge peak, a shifting ~ 0.7 eV up in energy is consistent with previous XANES observations for the presence of Fe species with higher valence state (i.e. 4+).[4,5] However, we note however, that the rising absorption edge is slightly red-shifted in comparison to what has been previously reported.[4,6] The reduction of the pre-edge peak on exposure to methane indicates a direct coordination of CH_4 with the Fe centre although a retention of this post activation state. It should be noted however that the position and intensity of the pre-edge peak (non sequitur, the edge position) is not a direct indication of oxidation state since the splitting and occupation of the 3d levels will affect the intensity as well as the 'real' electron density on the Fe site hence the difficulty in an unambiguous assignment of formal oxidation state. Exposure to H_2O_2 aqueous phase leads to a dramatic decrease in intensity consistent with increased coordination and restoration of the Oh Fe^{3+} containing species (Fig. S6b).
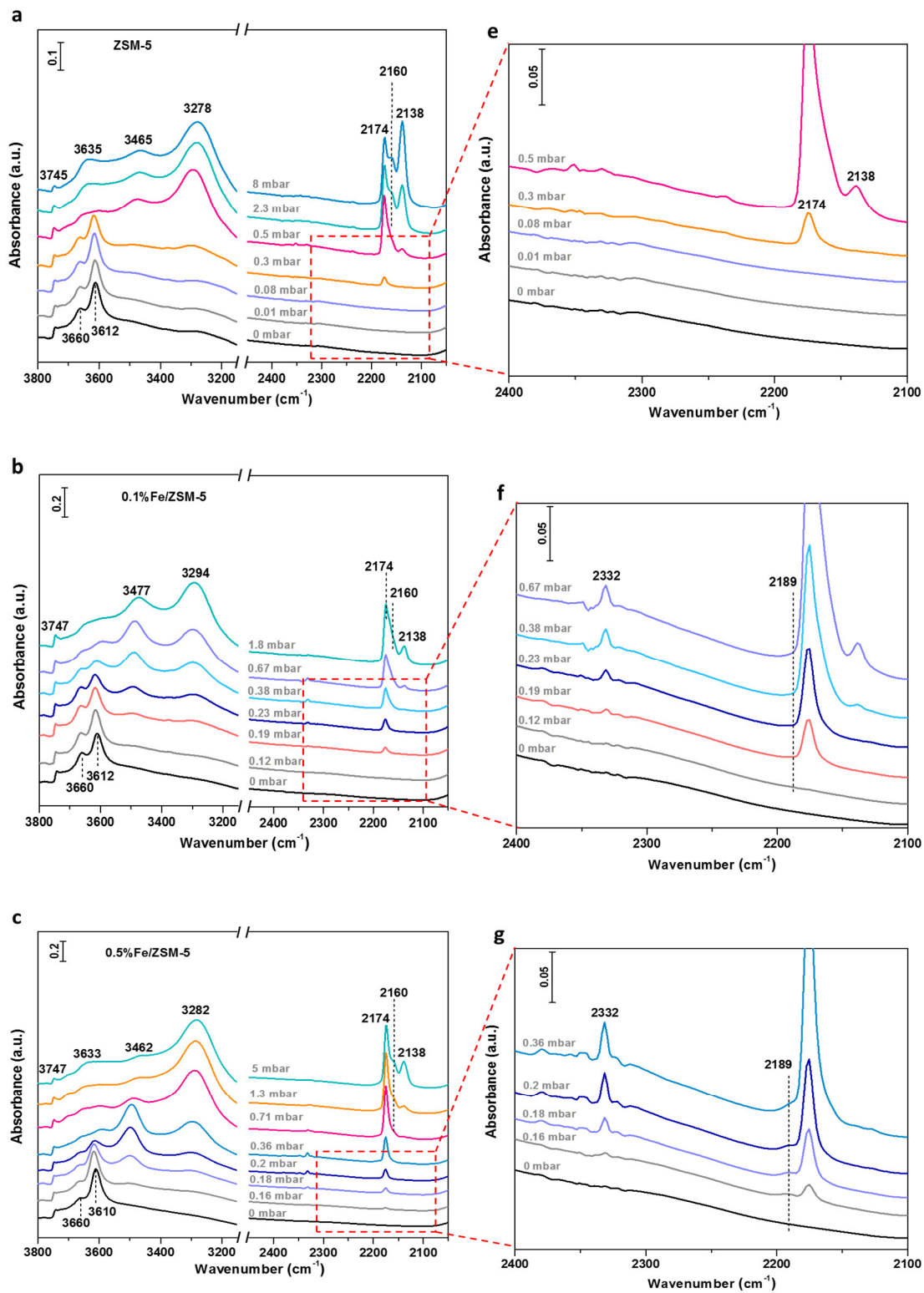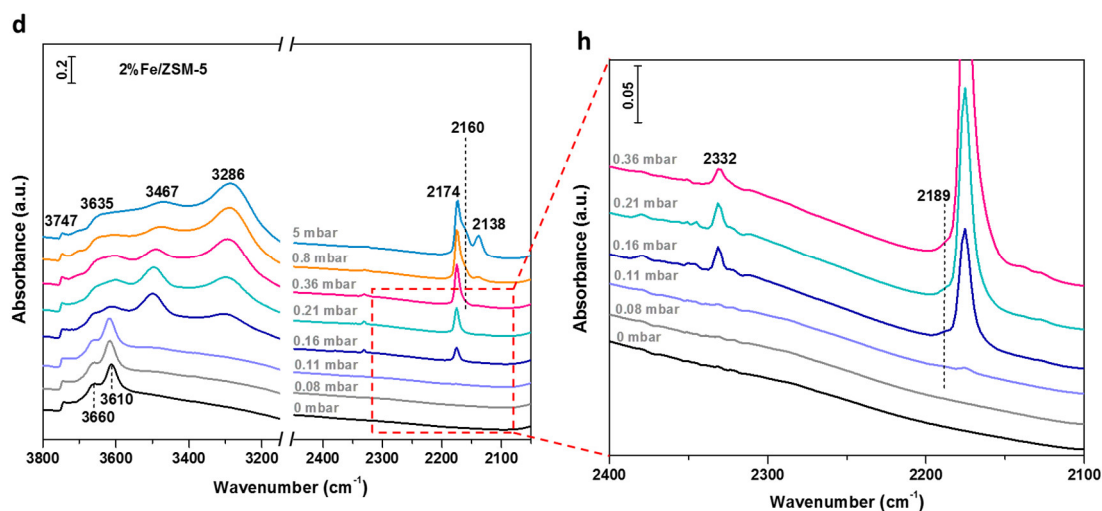
Figure S7. FT-IR spectra of CO stepwise absorbed at -190 °C on (**a**) ZSM-5, (**b**) 0.1%Fe/ZSM-5, (**c**) 0.5%Fe/ZSM-5 and (**d**) 2%Fe/ZSM-5, (**e-h**) enlargement of the corresponding spectra in box in **a**,**b**,**c** and **d**, respectively.

Note: The remarkable oxidizing prowess of Fe/ZSM-5 catalysts is supported by low-temperature infrared spectroscopy using CO as a probe molecule. The spectra of -OH stretching region of parent ZSM-5 and Fe/ZSM-5 catalysts with different iron loadings are shown in Fig. S7. Before the introduction of CO, three bands were observed at 3741, 3660 and 3612 cm^{-1}, assigned to Si-OH, Al-OH and Si-O(H)-Al (Brønsted acid sites),[7-10] respectively. After stepwise injection of CO, these three bands showed a red shift to 3633~3635, 3462~3477 and 3278~3294 cm^{-1}, owing to the interaction with CO. Additionally, two narrow bands at 2174 and 2138 cm^{-1} appeared for all the samples at high CO coverage, were assigned to CO adsorbed on the proton of the ZSM-5 and physically adsorbed CO. A broad band appears at 2160 cm^{-1}, could be attributed to a combing contribution of CO adsorbed on hydroxyl groups. Notably, via the enlargement of the corresponding spectra (Fig. S7e-h), two signals with weak intensity at 2189 and ~2332 cm^{-1} were detected for Fe/ZSM-5 samples at low CO coverage, which were absent in the parent ZSM-5 sample. The former one, according to previous data,[9,10] was assigned to CO adsorbed on extra-framework Fe^{2+} species; while the latter one was assigned to the asymmetric stretching vibration of CO_2. The formation of CO_2 and extra-framework Fe^{2+} species indicates the Fe^{3+} species in Fe/ZSM-5 catalysts to be strongly oxidizing, which enables the oxidation of CO to CO_2 even at -190 °C, in line with no detected CO in the gas phase for all the Fe/ZSM-5 catalysts. When considering the low loading of Fe and significant contribution of mononuclear Fe^{3+} species for methane oxidation, this excellent oxidation strength of Fe^{3+} is attributable to the presence of mononuclear Fe^{3+} species in Fe/ZSM-5 catalysts. Notably, the signal at 2189 cm^{-1} was observed with only limited intensity for 0.1%Fe/ZSM-5, owing to the low loading of Fe probably below the detection limit, making it difficult to be visualized by CO FT-IR.

Tables

Table S1. Comparison of catalytic performance for our catalysts and other reported catalysts.

Catalysts (Si/Al ratio)	Metal (wt%)	Temperature (°C)	Time (h)	Pressure (bar)	TOR* (h^{-1})	Ref.
Fe/ZSM-5 (13.5)	0.1	50	0.5	30	66	This work
	0.2	50	0.5	30	34	This work
	0.5	50	0.5	30	15	This work
	1	50	0.5	30	8	This work
	2	50	0.5	30	4	This work
FeN_4/GN	2.7	25	10	20	0.02	11
Fe/ZSM-5 (15)	2.5	50	0.5	30.5	4	12
Fe/ZSM-5 (15)	0.5	50	0.5	30.5	17	13
Fe/ZSM-5 (11.5)	2.5	50	0.5	30.5	8	14
Rh/ZSM-5 (15)	0.5	150	3	27†	14	15
Rh/ZrO_2	0.3	70	1	30	1	16
Cr/TiO_2	0.5	50	1	30	2	17
AuPd/TiO_2	1	70	0.5	30.5	0.4	18
AuPd@ZSM-5 (30)	5	70	0.5	30‡	14	19

*TOR is defined as mole (methanol) / mole (metal) / time.

†Reaction condition: 18.5% CO/7.4% O_2/74.1% CH_4.

‡Reaction condition: 3.3% H_2/6.6% O_2/1.6% CH_4/61.7% Ar/26.8% He.

Table S2. Properties of the catalysts studied.

Catalysts	Fe(wt%)*	Fe/Al ratio†	S_{BET} $(m^2 \cdot g^{-1})$	S_{micro} $(m^2 \cdot g^{-1})$‡	V_{total} $(cm^3 \cdot g^{-1})$	V_{micro} $(cm^3 \cdot g^{-1})$§
ZSM-5	0.03	0.005	326	244	0.21	0.131
0.1%Fe/ZSM-5	0.14	0.023	327	241	0.21	0.129
0.2%Fe/ZSM-5	0.25	0.041	317	237	0.20	0.127
0.5%Fe/ZSM-5	0.57	0.094	312	232	0.19	0.124
1%Fe/ZSM-5	1.10	0.181	296	227	0.18	0.123
2%Fe/ZSM-5	2.09	0.348	285	217	0.18	0.116

*Determined by ICP-OES.

†Fe contents were determined by ICP-OES, and Al contents were obtained from the molecular formula of $H_n[Al_nSi_{96-n}O_{192}] \cdot 16H_2O$.

‡, §Calculated by t-plot method.

Table S3. Summary of the Mössbauer parameters and assignments to different iron species in samples.

Catalyst	IS* (mm·s⁻¹)	QS† (mm·s⁻¹)	Area‡ (%)	Assignment
0.1%Fe/ZSM-5	0.36	0.70	66	Mononuclear Fe^{3+}
	0.34	1.55	34	Oligomeric Fe_xO_y cluster
0.2%Fe/ZSM-5	0.34	0.69	56	Mononuclear Fe^{3+}
	0.37	1.45	44	Oligomeric Fe_xO_y cluster
0.5%Fe/ZSM-5	0.36	0.67	43	Mononuclear Fe^{3+}
	0.37	1.45	42	Oligomeric Fe_xO_y cluster
	0.36	-0.29	15	Fe_2O_3 particle
1%Fe/ZSM-5	0.36	0.67	34	Mononuclear Fe^{3+}
	0.36	1.39	49	Oligomeric Fe_xO_y cluster
	0.38	-0.22	17	Fe_2O_3 particle
2%Fe/ZSM-5	0.35	0.65	28	Mononuclear Fe^{3+}
	0.36	1.07	57	Oligomeric Fe_xO_y cluster
	0.36	-0.23	15	Fe_2O_3 particle

Experimental uncertainties: ± 0.03 mm/s for IS and ± 0.07 mm/s for QS.

*Isomer shift, relative to α-Fe at room temperature.

†Quadrupole splitting, electric quadrupole splitting.

‡The relative absorption area of each iron species in Fe/ZSM-5 samples.

Table S4. Catalytic performance of methane oxidation over Fe/ZSM-5 catalysts.

Catalysts	CH_3OH (μmol)	CH_3OOH (μmol)	$HOCH_2OOH$ (μmol)	HCOOH (μmol)	CO_2 (μmol)	Conv.* (%)	C1 oxygenates sel.† (%)
H-ZSM-5	43	137	63	186	-	0.4	>99
0.1%Fe/ZSM-5	177	248	191	431	31	1.1	97
0.2%Fe/ZSM-5	178	234	205	779	65	1.5	95
0.5%Fe/ZSM-5	196	212	191	742	63	1.5	96
1%Fe/ZSM-5	217	210	172	1057	160	1.9	91
2%Fe/ZSM-5	214	182	207	1651	188	2.3	92

Reaction conditions: T = 50 °C, P_{CH4} = 30 bar, H_2O_2 = 0.5 M, catalyst = 0.3 g, rpm = 1500, V = 80 mL, t = 30 min. CH_3OH, CH_3OOH, $HOCH_2OOH$ and HCOOH were analyzed by ^1H NMR and CO_2 was analyzed by GC-TCD. *Conversion, calculated as (moles produced) / (initial moles methane)×100. †C1 oxygenates selectivity, calculated as (moles liquid products) / (moles produced)×100.

Note: Table S4 shows the yield of different products after methane oxidation over Fe/ZSM-5 with different iron loadings. Clearly, a trend that the yield of HCOOH and CO_2 increases with increasing Fe content of catalysts has been shown. The oligomeric Fe clusters and Fe_2O_3 particle species are more active for the overoxidation of methanol to formic acid and CO_2. This is consistent with previous reported results that the Fe oligomeric clusters and Fe_2O_3 aggregates in the Fe/ZSM-5 catalysts are more active in the unselective oxidation of the reductants.[20] The presence of Fe within the patent H-ZSM-5, as determined that concentrations as low as 0.03 wt% by ICP-OES, is pivotal for the activity, in line with the observation by previous reports.[12,13] However, the trace level of Fe is either near or beyond the detection limit of multiple characterization techniques (STEM, ^{57}Fe Mössbauer spectra, XAFS and FT-IR), leading to a significant challenge to identify the structure of existing species and to quantify each related portion.

Table S5. Fe K-edge EXAFS fitting results for 0.1%Fe/ZSM-5.

Sample	Shell	CN	R (Å)	$2\sigma^2$ (Å^2)	E_f (eV)	R_{factor}
Fresh	Fe-O	6.0±0.3	2.00	0.005	0±1	0.01
	Fe-Fe	0.8±0.4	3.06	0.008		
Dehydration	Fe-O	3.2±0.1	1.91	0.005	-4±1	0.01
	Fe-Fe	1.8±0.2	2.99	0.008		
CH$_4$ introduction	Fe-O	4.8±0.2	1.97	0.005	-4±1	0.03
	Fe-Fe	1.5±0.5	3.05	0.008		
H$_2$O$_2$(aq)	Fe-O	5.3±0.5	2.01	0.005	0±1	0.02
	Fe-Fe	1.0±0.5	3.03	0.008		

Note: Data for the fresh sample was recorded at ~298 K whilst all other data were recorded at 323 K. Hence the coordination number of Fe-O in the sample exposed to H$_2$O$_{2(aq)}$ can be considered ~6 since the Debye-Waller factor was constrained in the EXAFS refinement.

References

1 W. Luo, M. Sankar, A. M. Beale, Q. He, C. J. Kiely, P. C. A. Bruijnincx and B. M. Weckhuysen, *Nat. Commun.*, 2015, **6**, 6540.

2 M. Newville, *J. Synchrotron Radiat.*, 2001, **8**, 322–324.

3 B. Ravel and M. Newville, *J. Synchrotron Radiat.*, 2005, **12**, 537–541.

4 E. V. Kudrik, P. Afanasiev, L. X. Alvarez, P. Dubourdeaux, M. Clémancey, J. M. Latour, G. Blondin, D. Bouchu, F. Albrieux, S. E. Nefedov and A. B. Sorokin, *Nat. Chem.*, 2012, **4**, 1024–1029.

5 E. V. Kudrik, O. Safonova, P. Glatzel, J. C. Swarbrick, L. X. Alvarez, A. B. Sorokin and P. Afanasiev, *Appl. Catal. B*, 2012, **113**–**114**, 43–51.

6 J. J. Yan, T. Kroll, M. L. Baker, S. A. Wilson, R. Decréau, M. Lundberg, D. Sokaras, P. Glatzel, B. Hedman, K. O. Hodgson and E. I. Solomon, *Proc. Natl. Acad. Sci.*, 2019, **116**, 2854–2859.

7 M. Iwasaki, K. Yamazaki, K. Banno and H. Shinjoh, *J. Catal.*, 2008, **260**, 205–216.

8 M. Mihaylov, E. Ivanova, N. Drenchev and K. Hadjiivanov, *J. Phys. Chem. C*, 2010, **114**, 1004–1014.

9 K. Hadjiivanov, E. Ivanova, R. Kefirov, J. Janas, A. Plesniar, S. Dzwigaj and M. Che, *Microporous Mesoporous Mater.*, 2010, **131**, 1–12.

10 R. Kefirov, E. Ivanova, K. Hadjiivanov, S. Dzwigaj and M. Che, *Catal. Lett.*, 2008, **125**, 209–214.

11 X. Cui, H. Li, Y. Wang, Y. Hu, L. Hua, H. Li, X. Han, Q. Liu, F. Yang, L. He, X. Chen, Q. Li, J. Xiao, D. Deng and X. Bao, *Chem*, 2018, **4**, 1902–1910.

12 C. Hammond, M. M. Forde, M. H. Ab Rahim, A. Thetford, Q. He, R. L. Jenkins, N. Dimitratos, J. A. Lopez-Sanchez, N. F. Dummer, D. M. Murphy, A. F. Carley, S. H. Taylor, D. J. Willock, E. E. Stangland, J. Kang, H. Hagen, C. J. Kiely and G. J. Hutchings, *Angew. Chem. Int. Ed.*, 2012, **51**, 5129–5133.

13 C. Hammond, N. Dimitratos, R. L. Jenkins, J. A. Lopez-Sanchez, S. A. Kondrat, M. Hasbi ab Rahim, M. M. Forde, A. Thetford, S. H. Taylor, H. Hagen, E. E. Stangland, J. H. Kang, J. M. Moulijn, D. J. Willock and G. J. Hutchings, *ACS Catal.*, 2013, **3**, 689–699.

14 C. Kalamaras, D. Palomas, R. Bos, A. Horton, M. Crimmin and K. Hellgardt, *Catal. Lett.*, 2016, **146**, 483–492.

15 J. Shan, M. Li, L. F. Allard, S. Lee and M. Flytzani-Stephanopoulos, *Nature*, 2017, **551**, 605–608.

16 Y. Kwon, T. Y. Kim, G. Kwon, J. Yi and H. Lee, *J. Am. Chem. Soc.*, 2017, **139**, 17694–17699.

17 Q. Shen, C. Cao, R. Huang, L. Zhu, X. Zhou, Q. Zhang, L. Gu and W. Song, *Angew. Chem. Int. Ed.*, 2020, **59**, 1216–1219.

18 C. Williams, J. H. Carter, N. F. Dummer, Y. K. Chow, D. J. Morgan, S. Yacob, P. Serna, D. J. Willock, R. J. Meyer, S. H. Taylor and G. J. Hutchings, *ACS Catal.*, 2018, **8**, 2567–2576.

19 Z. Jin, L. Wang, E. Zuidema, K. Mondal, M. Zhang, J. Zhang, C. Wang, X. Meng, H. Yang, C. Mesters and F. S. Xiao, *Science*, 2020, **367**, 193–197.

20 M. S. Kumar, M. Schwidder, W. Grünert, U. Bentrup and A. Brückner, *J. Catal.*, 2006, **239**, 173–186.